PROCEEDINGS OF SPIE

SPIEDigitalLibrary.org/conference-proceedings-of-spie

SHARK-NIR on its way to LBT

L. Marafatto, E. Carolo, G. Umbriaco, M. Bergomi, D. Greggio, et al.

L. Marafatto, E. Carolo, G. Umbriaco, M. Bergomi, D. Greggio, F. Laudisio, L. Lessio, M. Montoya, K. Radhakrishnan, D. Ricci, D. Vassallo, M. Dima, S. Di Filippo, K. W. W. Don, V. Viotto, J. Farinato, "SHARK-NIR on its way to LBT," Proc. SPIE 12184, Ground-based and Airborne Instrumentation for Astronomy IX, 121843V (29 August 2022); doi: 10.1117/12.2629494

SPIE.

Event: SPIE Astronomical Telescopes + Instrumentation, 2022, Montréal, Québec, Canada

SHARK-NIR on its way to LBT

L. Marafatto[a,b], E. Carolo[a,b], G. Umbriaco[a,b,c], M. Bergomi[a,b], D. Greggio[a,b], F. Laudisio[a], L. Lessio[a,b], M. Montoya[d], K. Radhakrishnan[a,b], D.Ricci[a], D. Vassallo[a,b], M. Dima[a,b], S. Di Filippo[a,b], K.W. Don[d], V. Viotto[a,b], J. Farinato[a,b]

[a] INAF Osservatorio Astronomico di Padova, Vicolo dell'Osservatorio 5, 35122 Padua, Italy;

[b] ADONI - National Laboratory for Adaptive Optics, Italy;

[c] University of Padova, Dept. Physics and Astronomy, Vicolo dell'Osservatorio 3, 35122 Padua, Italy;

[d] University of Arizona, Steward Observatory, 933 N Cherry Ave, Tucson, AZ 85721, USA;

ABSTRACT

SHARK-NIR is a high contrast camera for the LBT, spanning the Y, J and H bands. It has been designed to fully exploit the high Strehl adaptive optics correction delivered by the FLAO module, recently upgraded to SOUL, and implements different coronagraphic techniques, with contrast as high as 10-6 up to 65 mas from the star. It also has spectroscopical capabilities, with low and medium resolution, and its relatively wide Field of View (18 x 18 arcsec) makes it accessible to other scientific targets, such as galactic jets and disks, as well as extra-galactic cases.

The nature of the instrument, requiring deep exploration of stars very close neighborhood, translates into the requirements of extreme delivered optical quality and stability, ideally not to degrade the exquisite correction performed by SOUL. To improve its performance, SHARK-NIR includes a couple of peculiar features, such as a fast internal TT loop to minimize the residual jitter and a local NCPA correction, performed through a DM inside the instrument itself. SHARK-NIR will be mounted at a gravity variant focal station, thus it has to cope with flexures, whose effects could kill the coronagraphic performance. To minimize the effect of flexures, SHARK-NIR is a very compact and stiff instrument, whose flexures have been characterized during a dedicated campaign in laboratory, where the whole instrument was mounted on a dedicated handling simulating different telescope elevations. We report here the main results of the flexures tests and of the AIV phase, ended at the beginning of 2022..

Keywords: SHARK, coronagraphy, flexures, NCPA

1. INTRODUCTION

SHARK [1] is an instrument proposed for the LBT[2] as one of the second generation instruments. It is composed by two channels: SHARK-VIS[3] , working from 0.4µm to 1µm, and SHARK-NIR[4] , working in the near infrared bands, Y, J and H, operating from 0.96µm to 1.7µm. SHARK-NIR is essentially an imager with coronagraphic capabilities, which can also exploit low resolution spectroscopy in coronagraphic fashion too. The instrument has been designed in order to respond to the requirements coming from challenging science cases, ranging from exoplanet search and characterization to star forming regions coronagraphic observations, where jets and disks will be explored in their innermost regions. In fact, the resolution achievable with a 10- m class telescope allows to access, in the NIR domain, gaseous giant planets of Jupiter size or bigger, which still is a very challenging task to be achieved, due to the very high contrast and vicinity to the hosting star required. To achieve such a high contrast, it is mandatory an AO system performing an extreme correction, which is the case of LBT, thanks to the performance of both the wavefront sensor (FLAO[5], based on the Pyramid[6] WFS) and the DM Adaptive Secondary Mirror ASM[7]), which can be seen in the impressive collection of observations with FLAO shown in Figure 1, in terms of Strehl Ratio . Such a very good performance will be further improved with the implementation of the AO upgrade SOUL (Single Conjugated Adaptive

Ground-based and Airborne Instrumentation for Astronomy IX, edited by Christopher J. Evans, Julia J. Bryant, Kentaro Motohara, Proc. of SPIE Vol. 12184, 121843V
 · 0277-786X · doi: 10.1117/12.2629494

Optics Upgrade for LBT), giving the capability to achieve SRs as high as 70% at magnitudes >13 (see [9]). We recall in fact that the Pyramid WFS has a demonstrated gain in sensitivity compared to other WFSs commonly used, such as the Shack-Hartmann ([10], [11], [12], [13], [14]), currently implemented in SPHERE[15] and GPI[16]. This fact allows LBT AO systems to achieve high SR (of the order of 70%) also at moderately faint magnitude (R~12 or even occasionally fainter, depending on the observing conditions), giving the possibility to increase the sample of stars to be observed, allowing deep search for planets around targets like, e.g., M dwarfs in nearby young associations and solar type stars in nearby star-forming regions (Taurus-Auriga at 140 pc). Also in the extragalactic field, the sample of AGN and, above all, of Quasars to be explored will go from a few tenths to a few hundreds, changing the perspective of the science to be achieved and giving to SHARK-NIR unique opportunities in the coronagraphic instrument scenario.

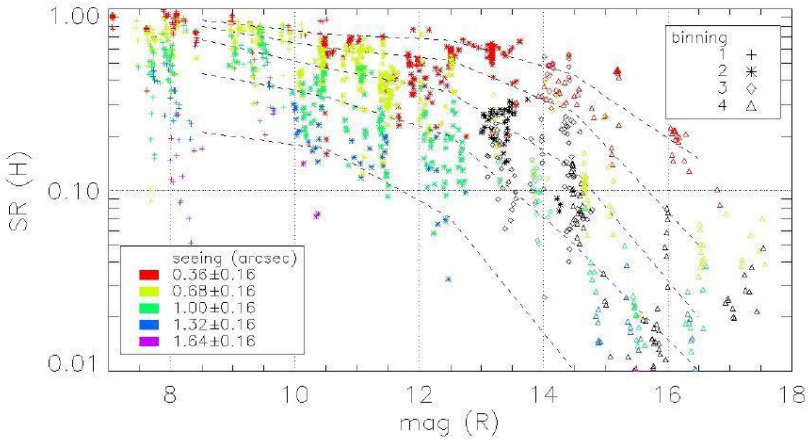

Figure 1: a summary of the FLAO performance obtained in H band with different observing conditions

Another unique characteristics of LBT is the possibility to make contemporary coronagraphic observations with three instruments: SHARK-NIR on one arm, operating between Y and H bands and SHARK-VIS (B,V,R I and Z bands) and LMIRcam (the infrared camera of LBTI[8], observing in K, L and M bands) on the other arm, which can make contemporary observations since the light is split between the two instruments with a dichroic. Such a capability is unique in the contest of the planet finders currently operating on sky. SHARK-NIR is currently toward the end of the AIV phase, to be soon installed at LBT. In the following sections we briefly describe the instrument and we present the AIV activities performed in the laboratories of the INAF-Astronomical Observatory of Padova.

2. INSTRUMENT DESCRIPTION

SHARK will be installed at the entrance foci of LBTI (LBT Interferometer), as it is shown in Figure 3, using two deployable dichroics to feed the two SHARK channels. In this way, on the VIS side, the IR light is totally transmitted to LBTI, while on the NIR side, the NIR light will be sent to SHARK-NIR. The dichroics is positioned just before the entrance window of LBTI, the latter transmitting the IR light to the interferometric focus and reflecting the VIS light to the Pyramid WFS . The dichroic of the VIS channel will pick-up only a certain amount (selectable) of the VIS light, to feed with the rest the WFS, while the one of the NIR channel will pick up up only the Y, J and H bands, letting all the visible light going through to the WFS. With this setup, SHARK will provide possible contemporary observations with three instruments at the same time from R to K bands. Such a flexible configuration with several combined binocular observing modes is reflecting the request coming from the principal science cases, for which simultaneous observations in the VIS and NIR domain are required. SHARK-NIR is a camera for direct imaging coronagraphy and spectroscopy, which is taking advantage of the existing LBT AO systems, based on the LBTI AO WFS and on the Adaptive Secondary Mirror (ASM).

The instrument is designed to achieve an intrinsic extreme performance, not to decrease the correction provided by the AO system, since all the coronagraphic techniques need a SR as high as possible to provide contrasts as high as possible. This requires optics characterized by a very good optical quality, meaning machined to a state of the art technology and polished to nanometric level of roughness, properly aligned and installed on very robust mounts. The whole instrument mechanics has to be very stiff and designed to minimize the effects of flexures. We also implemented an atmospheric dispersion corrector (ADC) to compensate for the atmospheric dispersion, in order to maintain the performance as good as possible at every observing altitude. To accomplish the field de-rotation required by some of the foreseen science cases, the whole instrument is mounted on a mechanical bearing, clearly visible in Figure 4. The NIR scientific camera is based on an Teledyne H2RG detector, cooled at about 80°K to minimize the thermal background. It will provide a FoV of the order of 18"x18" operating in Y, J and H bands, with a plate scale foreseeing a bit more than two pixels on the diffraction limit PSF at 0.96μm.

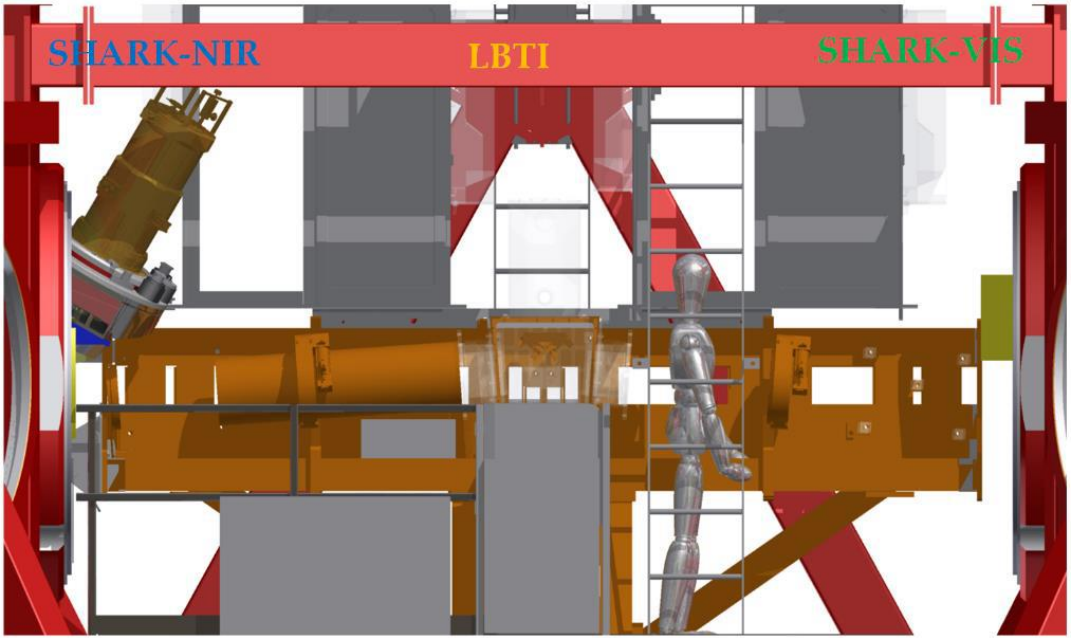

Figure 2: the two SHARK channels installed at the LBTI entrance foci

A few subsystems have been introduced in the instrument design with the purpose of optimizing the instrument performance. SHARK-NIR includes a couple of very important sub-systems which have been introduced with the purpose of optimizing the instrument performance and maintaining it at least on the time scale of the scientific exposure. For the Non-Common Path Aberrations (NCPA) minimization, a local DM (ALPAO DM 97-15) has been introduced into the first pupil plane, allowing a local removal of the aberrations. The same DM, used in Tip-Tilt (T-T) fashion, may be used to correct undesired PSF movements during a scientific exposure, essentially due to the residual jitter. The latter correction requires a dedicated T-T sensor (based on the First Light C-RED2 camera), which has been placed after the first pupil plane, where a beam splitter positioned into the collimated beam picks-up few percent of the light (10%) and sends it to the sensor. A Wave Front Computer (WFC, which is realized by Microgate) allows the fast T-T correction achieved with the DM, which maintains at the same time the proper shape for the Non Common Path Aberrations (NCPA) local compensation. There is also a filter wheel between the DM and the beam splitter feeding the T-T sensor, positioned at 50mm from the pupil plane, which carries the apodizing masks. These kinds of masks are normally placed exactly into the pupil plane, which is occupied by the DM in our design. We did evaluate the impact of having the masks slightly displaced with respect to the pupil plane, and the effect is basically negligible with the considered coronagraphic techniques if the masks are designed to take this fact into account. Concerning coronagraphy, we decided to implement the following techniques, accordingly to the requirements of the different science cases in terms of contrast and Inner Working Angle:

- Gaussian Lyot, which needs a gaussian stop into the 1st focal plane and a pupil stop on the 2nd pupil plane
- Shaped Pupil, which needs an apodizing mask into the 1st pupil plane and an occulting mask into the 1st focal plane
- Four Quadrant, which requires a "knife edge" like mask into the 1st focal plane and a pupil stop on the 2nd pupil plane

3. INSTRUMENT FLEXURES TEST

Being SHARK-NIR an instrument installed at a gravity variant focal station, and being the field de-rotation obtained by making rotating the whole instrument, mechanical flexures will play an important role in the instrument performance. The instrument has been designed from the beginning in order to be compact, light and stiff, so to be less prone to flexures. A FEA analysis has been performed, and its result analyzed, in order to identify possible effects on stability of SHARK-NIR focal planes and pupil planes when the orientation of the instrument w.r.t. the gravity vector varies.

We performed several tests on the instrument to compare the results from the analysis with actual results coming from our tests. First of all, we distinguish between the two different regimes SHARK-NIR can experience: Field-stabilized and pupil-stabilized modes. In field-stabilized mode, the bearing rotates following the sky, and it can rotate up to 90° during a single exposure. At the same time the telescope changes its elevation to track scientific object. In pupil-stabilized mode, SHARK-NIR bearing is steady, and the only flexures come from the telescope changing its elevation. These tests have been performed with SHARK-NIR mounted on a big motorized bearing to simulate a telescope changing elevation. Shift of focal planes can be a performance killer for SHARK-NIR, especially when used for coronagraphic observations. Since fast tip-tilt loop will be running, flexures at the level of the technical camera (TECCAM) will be compensated by the loop, which will keep the TECCAM focal plane steady within some residual. It is thus very important to understand the relative shifts between TECCAM FP, Coronographic FP and Scientific FP. To perform flexures test, SHARK-NIR was fully mounted on a big derotator, whose rotation reproduces an elevation change of the telescope.

We had different sources to run this test:

- Internal calibration fiber (in focus), used to acquire internal reference PSF and internal pupil images. Light from this source passes through all the optics of SHARK-NIR but the dichroic and the IN-TT.

- Telescope simulator source, used to acquire a PSF and telescope pupil. Light from this source passes through all the optics of SHARK-NIR, included the dichroic and the IN-TT.

- Internal integrating sphere, used to illuminate the focal plane masks with an extended source, in order to measure the position of the occulting masks center and compare it with the PSF center.

- The internal calibration fiber is located at the entrance focal plane of the instrument, and it is deployed to acquire:

- Images of internal PSF, useful to check the effect of flexures internal to SHARK-NIR optical bench + SCICAM.

- Images of the internal pupil.

- Images of the apodizing masks (positioned at 50 mm from the 1st pupil plane).

- Phase diversity images, to verify the evolution of the NCPA at different telescope elevations.

The telescope simulator source is substantially a diffraction limited fiber, fed with broadband VIS and NIR light, whose light is collimated by a commercial OAP. In the telescope simulator pupil plane, there is a mask resembling the LBT single arm pupil, including the ASM swing arm shape, and finally a commercial lens focuses the light in a F/15 beam at the entrance focal plane of SHARK-NIR. Since the light from the telescope simulator passes through the SHARK-NIR optics on the deployable arm (the dichroic and the IN-TT), it is deployed to acquire:

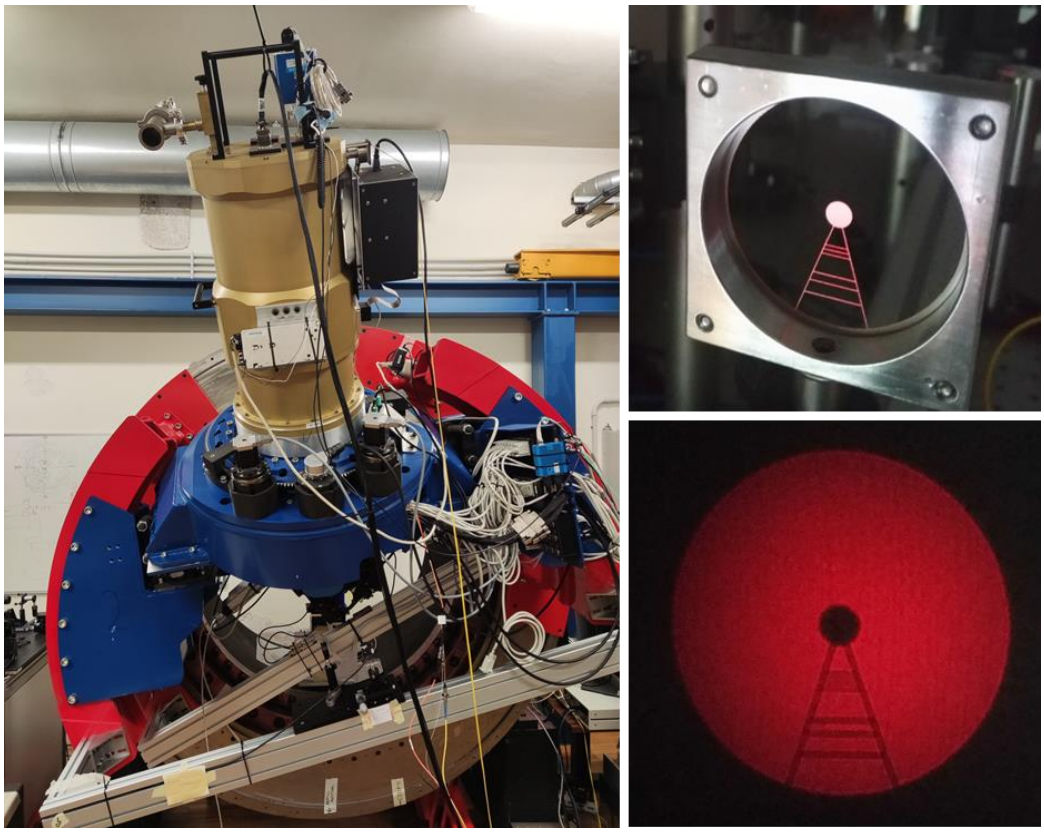

Figure 3: SHARK-NIR connected to the telescope simulator (left side) and the pupil mask simulating the LBT spider arm (right side)

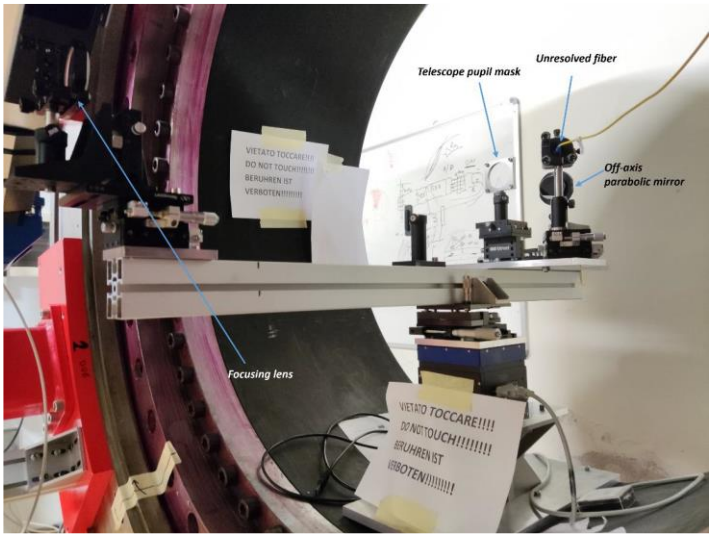

Figure 4: the telescope simulator used for the flexures tests.

Images of the telescope simulator PSF. Its position is affected by SHARK-NIR optical bench flexures, as the PSF from the calibration fiber, from the flexures of the deployable arm and from mis-alignment of the deployable arm optics (telescope simulator PSF not conjugated to the bearing rotation axis). It shall be considered that, when the fast tip-tilt loop is running, the effect of all the flexures happening before the

TECCAM are corrected, at the focal plane, by the loop. This means that flexures of the deployable arm will mainly affect the position of the pupil, which is not monitored and corrected during observation, and slightly the optical quality of the PSF, but not the PSF position w.r.t. the focal plane masks.

Images of the telescope pupil, useful to see how it will wobble during an observation due to flexures. However, the telescope simulator chief ray was aligned to the SHARK-NIR bearing rotation axis by minimizing the pupil wobble, observed on the SCICAM, on a 180 deg bearing rotation. The flexures of the SCICAM for a 180 deg bearing rotation are significant, thus the alignment of the telescope simulator chief ray is somehow compensating SCICAM flexures. As a result, the chief ray is not perfectly aligned to the bearing rotation axis (**for the future, align the telescope pupil to be perfectly cocentered to the internal pupil, rather than minimizing the wobble)**. For this reason, to compare relative wobble between pupil image and pupil plane masks, the pupil generated with the calibration fiber has been preferred as a reference. Shift of the telescope pupil at different telescope elevation has been explored during tests described in Section 6.2, while the effect of SHARK-NIR bearing rotation is basically the same on internal pupil and telescope simulator pupil, as the deployable arm is steady when SHARK-NIR bearing rotates. Moreover, during a scientific observation, the telescope elevation is expected to change by maximum 5 deg, and at the end of observation the pupil position can be checked again and re-adjusted, if necessary.

The integrating sphere source was fed by broadband VIS and NIR light, and its light is focused by an optical relay at the entrance focal plane of SHARK-NIR, providing a focused image of an extended (more than the scientific FoV of SHARK-NIR) object. It is deployed to acquire:

Images of the focal plane masks, useful to check the effect of flexures on their position with respect to the PSF star during an observation (due basically to the differential flexures between the coronagraphic focal plane and the TECCAM focal plane, where the fast tip-tilt loop is closed).

Images of the Lyot stop masks at the 2nd pupil plane. Ideally, one could have used the calibration fiber to acquire these images (similarly to what has been done for the apodizing masks). We chose to use this light source cause, differently from the apodizing masks, the Lyot stop masks are located exactly on the pupil plane. Thus, even if we are illuminating the masks from many direction, we still get a sharp image of the masks. Technically, this should be the case also using the calibration fiber (illuminate the pupil from a single direction), but our calibration fiber has a baffle which is physically blocking part of the emitting light to select a F/15 beam. The baffle is acting as a stop and the SCICAM is not conjugated to the position of the baffle, and this results in blurred images of the pupil, with also some diffraction effect.

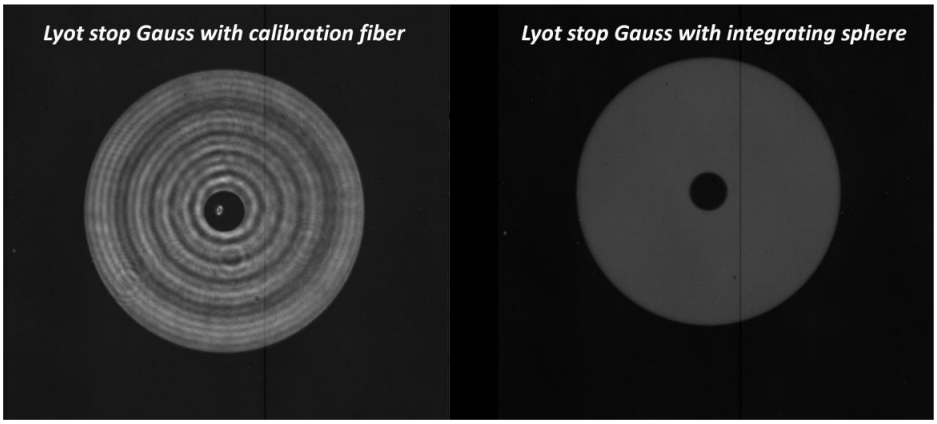

Figure 5: Lyot stop mask images taken with different illumination sources.

This test has been performed in two fashions:

- In open loop, meaning that the fast tip-tilt loop was not active. This is NOT how the instrument will operate at the telescope. Using the internal calibration fiber as a source instead of the telescope simulator allow us to understand the effect of the optical bench internal flexures on the PSF and pupil position w.r.t. the coronagraphic masks. It neglects the effect of flexures of the deployable arm and its mis-alignment w.r.t. the bearing rotation axis. However, this is almost steady during a bearing rotation, with a maximum expected change in the telescope elevation of 5 deg during a scientific observation. The effect of such a variation are explored during the test in pupil stabilized mode. For this reason, for the open loop tests we only considered the data acquired with the internal calibration fiber.
- In closed loop, meaning the fast tip-tilt loop was active. This is how the instrument will operate at the telescope. The loop keeps the focal plane almost fixed, regardless from common flexures and misalignment of the input source w.r.t. the bearing rotation axis. Only differential flexures between the TECCAM focal plane, where the loop is closed, and the CORO focal plane may impact the instrument performance. For this reason, in this configuration we used the telescope simulator PSF as a source to investigate focal plane movement. For the pupil shift, we kept using the internal pupil, as we do not have a control loop for the pupil, thus its shift during a bearing rotation would be affected by misalignment of the chief ray w.r.t. the bearing rotation axis.

For the open loop tests, we acquired images of the coronagraphic masks CORO and LYOT (not APO, as they will not be used in field stabilized mode), of the internal PSF and pupil at the following bearing angles:

- 131 deg
- 161 deg
- 191 deg
- 221 deg
- 251 deg
- 281 deg
- 311 deg

All these measurements have been repeated at the following telescope simulator elevations:

- 0 deg
- 5 deg
- 10 deg
- 15 deg
- 20 deg
- 30 deg
- 45 deg
- 60 deg

Spanning the whole operative range of SHARK-NIR, both in terms of bearing rotation and telescope elevation.
For the focal plane mask it is very important to understand what is the differential shift between the star PSF and the center of the occulter, as misalignment would cause light spilling out of the mask thus decreasing the contrast. All the focal plane masks showed basically the same behavior during a bearing rotation, so we show here, as representative of all the coronagraph, the differential movement of the internal PSF w.r.t. the FQPM. We chose this mask cause the algorithm to compute its center is more precise (± 0.1 pix) than the ones we use for the other masks.

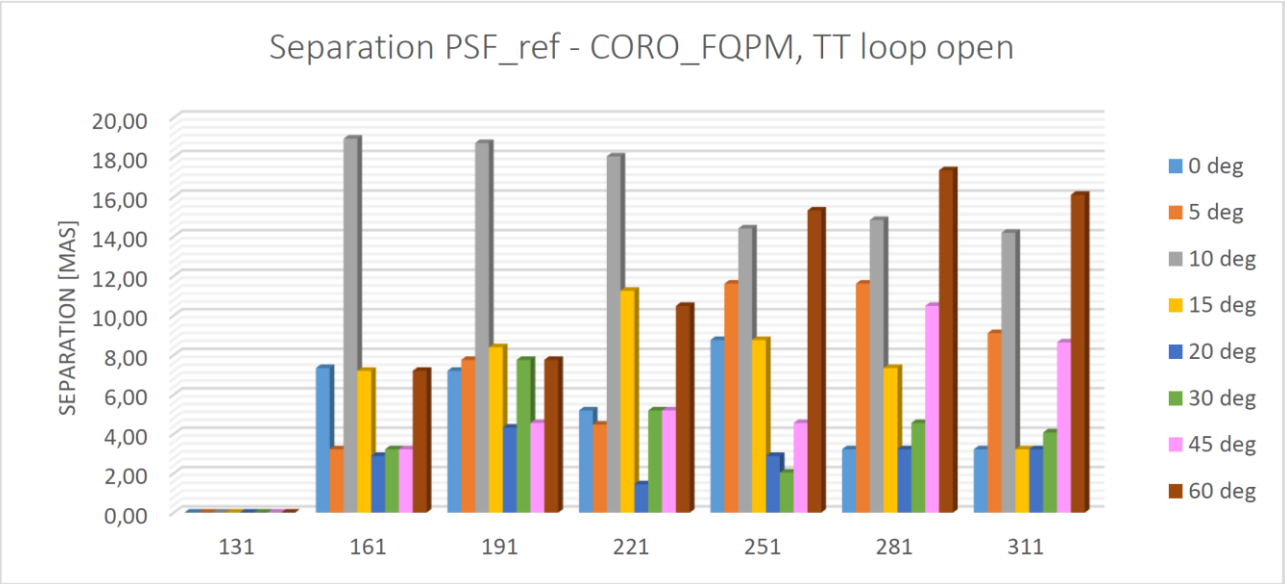

Figure 6: separation between the calibration fiber PSF (simulating a star) and the center of the FQPM, as observed on the SCICAM, at different bearing angle positions and telescope elevations.

Table 1: differential shift, in mas on sky, between the fiber PSF and the FQPM focal plane mask. Highlighted in red, the worst separation.

		Telescope elevation							
		0	**5**	**10**	**15**	**20**	**30**	**45**	**60**
Bearing rotation	**131**	0	0	0	0	0	0	0	0
	161	7.3	3.2	18.9	7.2	2.9	3.2	3.2	7.2
	191	7.2	7.8	18.7	8.4	4.3	7.8	4.6	7.8
	221	5.2	4.5	18.0	11.3	1.4	5.2	5.2	10.5
	251	8.8	11.6	14.4	8.8	2.9	2.0	4.6	15.3
	281	3.2	11.6	14.8	7.3	3.2	4.6	10.5	17.3
	311	3.2	9.1	14.2	3.2	3.2	4.1	8.6	16.1

For the pupil shift it is very important to understand the differential movement between the pupil and the Lyot stops (apodizing masks are NOT used in field stabilized mode), considering that a misalignment of 1% of the pupil diameter has a negligible effect on the raw contrast. For this test we have used the internal pupil, which is not affected by misalignment w.r.t. the bearing rotation axis effects. In this way we are neglecting the effect of the deployable arm flexures, but this is a second order effect, as the elevation of the telescope will change very slowly during a scientific observation (and will change slower at sky position requiring a fast derotation).

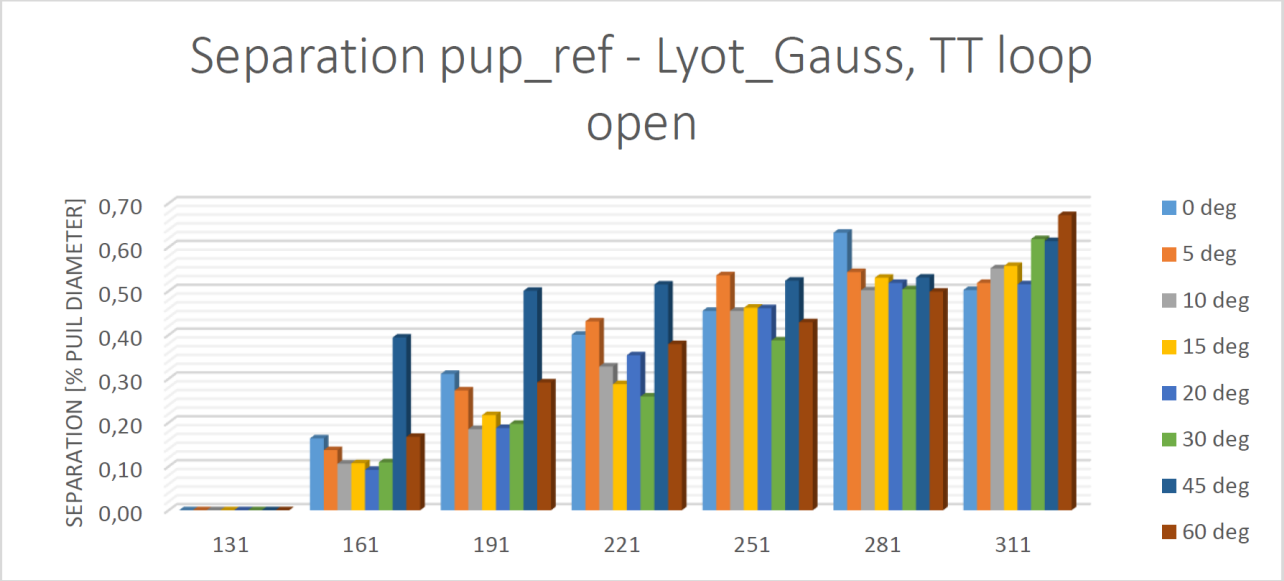

Figure 7: separation between the calibration fiber pupil and the Gauss Lyot stop, as observed on the SCICAM, at different bearing angle positions and telescope elevations.

Table 2: differential shift, in % of pupil diameter, between the fiber pupil and the Gauss Lyot stop mask. Highlighted in red, the worst separation.

		Telescope elevation							
		0	**5**	**10**	**15**	**20**	**30**	**45**	**60**
Bearing rotation	**131**	0	0	0	0	0	0	0	0
	161	0.16	0.14	0.11	0.11	0.09	0.11	0.39	0.17
	191	0.31	0.27	0.18	0.22	0.19	0.20	0.50	0.29
	221	0.40	0.43	0.33	0.29	0.35	0.26	0.51	0.38
	251	0.45	0.54	0.45	0.46	0.46	0.39	0.52	0.43
	281	0.63	0.54	0.50	0.53	0.52	0.50	0.53	0.50
	311	0.50	0.52	0.55	0.56	0.52	0.62	0.61	0.67

3.1 Flexures tests in pupil stabilized mode

In pupil stabilized mode, the SHARK-NIR bearing is steady and the telescope is changing its elevation. In this configuration the maximum change in elevation during a scientific exposure is assumed to be 5 degrees.

It is then very important to understand the differential movement of the source w.r.t. the occulter and of the telescope pupil w.r.t. the pupil masks for each 5deg telescope elevation variation, as mis-alignment would result in contrast loss. Also, it is important to characterize the common shift of the focal plane and pupil plane for a 5deg variation of telescope elevation, as a big movement during the observation would result in a blurred or swiped image of the object.

In pupil stabilized mode, the object is observed while it is crossing the meridian, to minimize the evolution of the quasi-static speckles, in particular for ADI post processing on exoplanets images, which is SHARK-NIR main scientific target. For this reason, we analyzed the movement of all the coronagraphic masks and of PSF and pupil with a telescope elevation sampling of 5deg in from the zenith to 35 deg, then at 45 deg and at 60 deg.

The images of focal plane masks and PSF have been acquired on the SCICAM in 128x128 pixels windowing, while pupil plane masks images in 2048 x 1280 pixels windowing.

Images were acquired with the fast TT loop closed at 1 kHz, to mimic the working condition at the telescope.

Figure 8 shows the differential shift, given in *mas* on sky, of the PSF coming from the telescope simulator and of the FQPM occulting mask, for a given Δ-elevation of the telescope. For this test, the FQPM is taken as representative of the movement of all the focal plane coronagraphic masks for two reasons:

- From other tests shown in the next pages, the differential movement of the FQPM and Gaussian occulter is basically negligible.

- The algorithm to calculate the FQPM center has a better accuracy (0.1 px vs 0.5 px) than the algorithms used to calculate the center of the Shaped pupils occulters.

The maximum differential shift between telescope PSF and FQPM is 6.11 *mas*, while the worst case result coming from the FEA, reported in AD1, is 5.9 *mas*.

The maximum shift of the telescope PSF on the SCICAM for a 5 deg telescope elevation variation is 9.22 mas (see *Figure 9*), not comparable with a FEA as it was not available for the SCICAM. For images requiring a higher stability of the image, a reference source in the image will be necessary to perform shift & add (spots generated through the Fourier modes can be used for this purpose).

Figure 10 shows the differential shift, given in *%* of the pupil diameter, of the telescope pupil and of the apodizer SP2a mask, for a given Δelevation of the telescope. Apodizer SP2a is taken as representative of the movement of all the apodizing masks, as the differential movement between these masks is negligible. The same applies to *Figure 11*, referring to Lyot stop for the Shaped Pupils.

The maximum differential shift between telescope pupil and apodizer SP2a for a 5 deg telescope elevation variation is 0.25% of the pupil diameter, while the apodizing masks pattern are oversized by 0.5% of the pupil diameter.

The maximum differential shift between telescope pupil and Lyot SP mask for a 5 deg telescope elevation variation is 0.23% of the pupil diameter, while the Lyot masks tolerates a shift of the telescope pupil of the 1% of the pupil diameter.

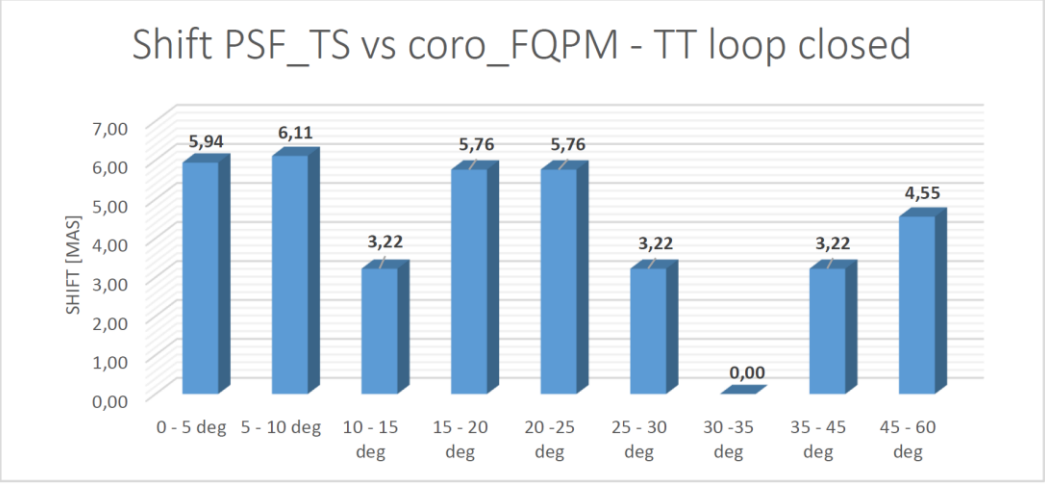

Figure 8: differential movement between the PSF from the telescope simulator and the FQPM occulting mask for different variation of telescope elevation. Shifts are given in mas on sky.

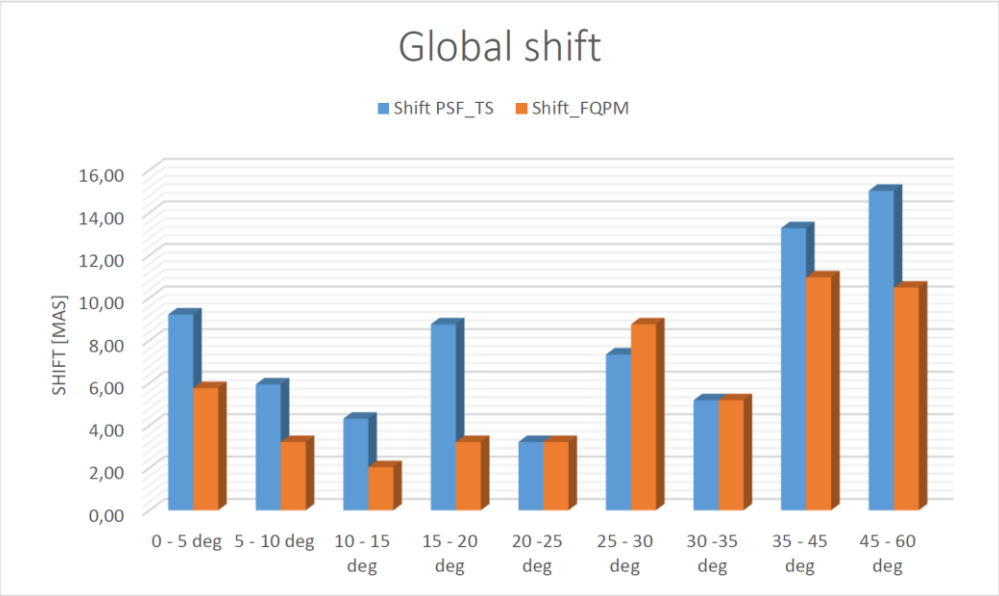

Figure 9: global shift of the PSF from the telescope simulator and of the FQPM on the SCICAM for different telescope elevations. Shifts are given in mas on sky.

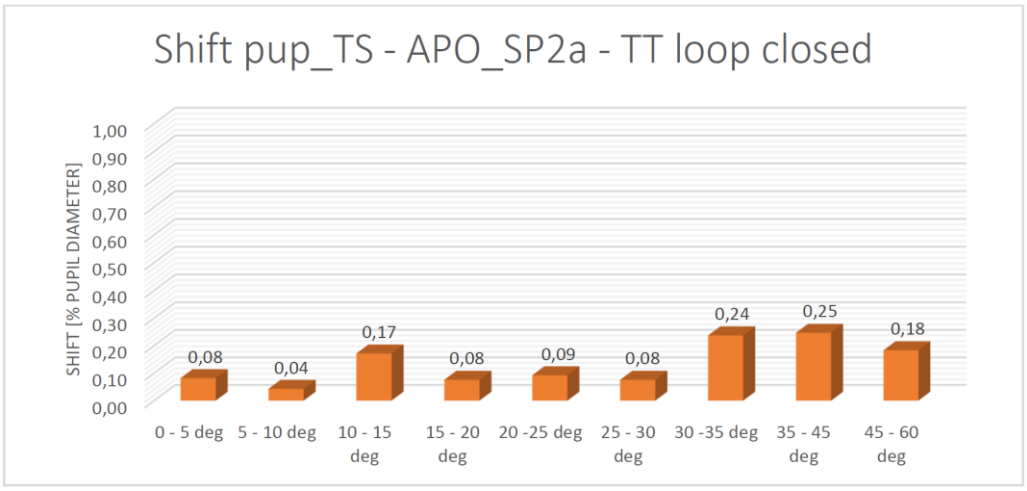

Figure 10: differential movement between the telescop pupil and the apodizer SP2a mask for different variation of telescope elevation. Shifts are given in % of the pupil diameter.

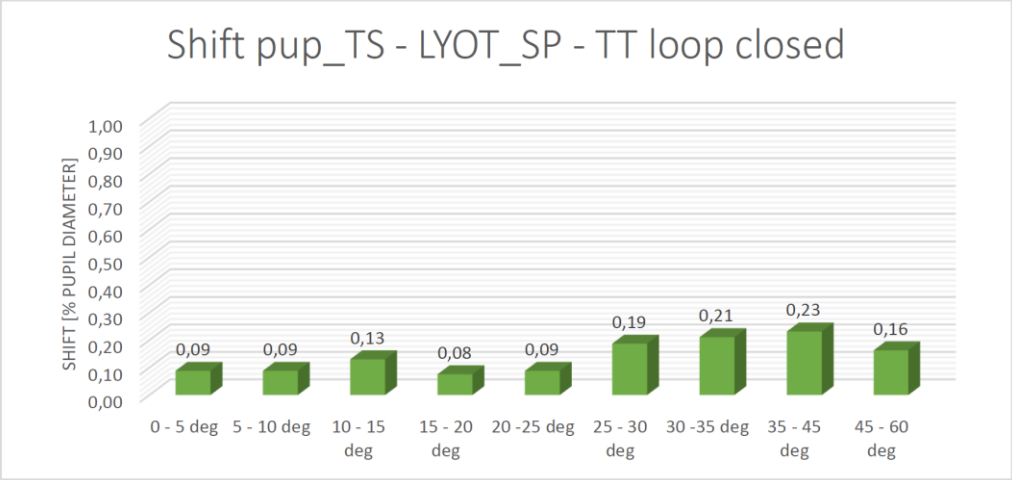

Figure 11: differential movement between the telescope pupil and the Lyot SP mask for different variation of telescope elevation. Shifts are given in % of the pupil diameter.

3.2 Summary of flexures test

In *Table 3* are summarized the main results from flexures tests, both in field stabilized and in pupil stabilized fashion, and the worst obtained results are compared with expectations from FEA analysys.

Table 3: the results of the flexure test in terms of PSF and pupil shifts everywhere "on sky": the worst values obtained during the test are reported in the tables

Pupil stabilized mode		
	Requirement/FEA	Flexures test results
Differential shift PSF – CORO masks	6 mas	6.11 mas
Differential shift pupil – APO masks	0.5% pupil diameter	0.25% pupil diameter
Differential shift pupil – Lyot masks	1% pupil diameter	0.23% pupil diameter

Field stabilized mode		
	Requirement/FEA	Flexures test results
Differential shift PSF – CORO masks	30 mas	19 mas
Differential shift pupil – Lyot masks	1%	0.67% pupil diameter

4. FAST TIP-TILT LOOP

Important results from past tests was that we could not achieve the required correction residual for stars fainter than 11th magnitude, due to the RON of the technical camera. We then decided to change the beam splitter folding light to the technical camera from a 5/95 R/T to a 10/90 R/T, taking some light from the scientific channel to match the correction residual requirement.
Here are presented the results obtained with the new beam splitter. All the tests have been performed on the final system. The AO-channel has been characterized both to quantify the efficiency of the residual tip-tilt correction against the star R-magnitudes and the loop frame rates (500 and 1000 Hz), introducing a Tip Tilt history disturbance directly to the DM with different residual jitter amplitudes (15, 10 and 5 mas rms). *Table 4* summarizes the results obtained from the lab experiment, showing that the loop is able to reduce the residual jitter of about a factor 5 in the best cases, and still at magnitude 12 there is a reduction of about a factor 2. 15mas RMS of residual jitter to be corrected is an extremely conservative case, as the jitter of the star should be already corrected by AO and we expect a residual jitter more of the order of 5 mas.

Table 4: results of fast tip-tilt loop for different input jitter, star magnitude and loop clock. In green the results within the requirement. In light red results with a Δ < 10% from to requirement. In red results not in requirement.

R magnitude	Input time history / Frame Rate [Hz]	15 mas	10 mas	5 mas	Requirement SDA-01
Mag 9	2000	2.7	2.3	2.2	5
Mag 10	1000	4.2	3.0	2.3	5
	2000	4.2	4.0	3.9	5
Mag 11	500	4.8	4.2	3.0	5
	1000	4.9	3.8	3.3	5
Mag 12	500	7.3	5.3	3.7	5

5. CORONAGRAPHIC MASKS ALIGNMENT

In order not to degrade the coronagraphic performance of the instrument, the psf from the star has to be aligned with very high precision to the occulting mask, while the pupil of the telescope has to be aligned with the pupil plane masks.
For this reasons we implemented very precise algorithm to calculate the center of the coronagraphic masks. These algorithms are included in some automatic alignment procedures which take care of measuring automatically the position of the pupil plane masks, focal plane masks, telescope pupil and PSF and to co-align them within a certain threshold, specified by the user.

5.1 Alignment routine pupil telescope to apodizers

This routine automatically acquire an image of the telescope pupil and of the apodizing mask/Lyot stops that will be used for the observation, and compute center and orientation of both of them. Acting on the bearing rotation and on the tip-tilt of the IN-TT mirror of SHARK-NIR, the telescope pupil position and orientation will be adjusted till the two images will be:

- Co-centered better than Δx: 1px, Δy: 1 px, in case of alignment of the pupil to the apodizing masks. In distance corresponds to a worst case of 1.4px ~ 0.2% of the pupil diameter.

- Co-centered better than Δx: 3px, Δy: 3 px, in case of alignment of the pupil to the Lyot stops. In distance corresponds to a worst case of 4.2px ~ 0.6% of the pupil diameter.

- Co-oriented better than 0.5°

This routine has been extensively tested in the lab, using as a source a telescope simulator including a mask closely resembling the LBT pupil (photolithographic mask).

Requirement for centering telescope pupil to apodizing mask residual is 0.4% of pupil diameter. Requirements for centering to the Lyot stops is much looser, as the FQPM Lyot stop, which has the tightes tolerances among the Lyot stops, well tolerates mis-alignments up to 1% of the pupil diameter.

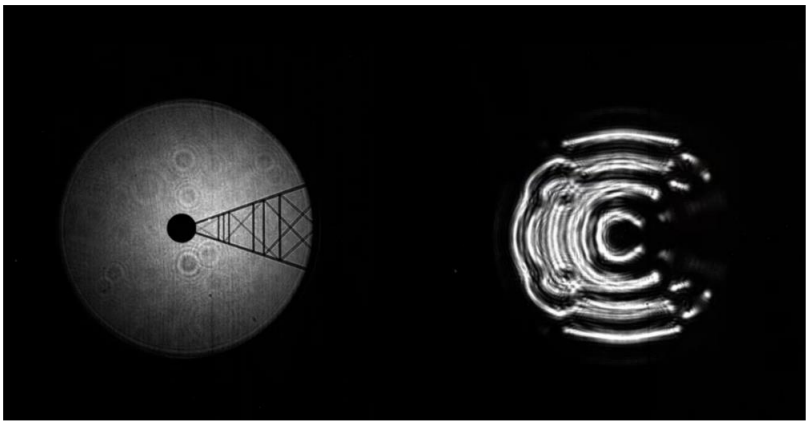

Figure 12: left panel, an image of the telescope pupil mask included in the telescope simulator, as seen by SHARK-NIR. Right panel, an image of SP1 apodizing mask, as seen by SHARK-NIR.

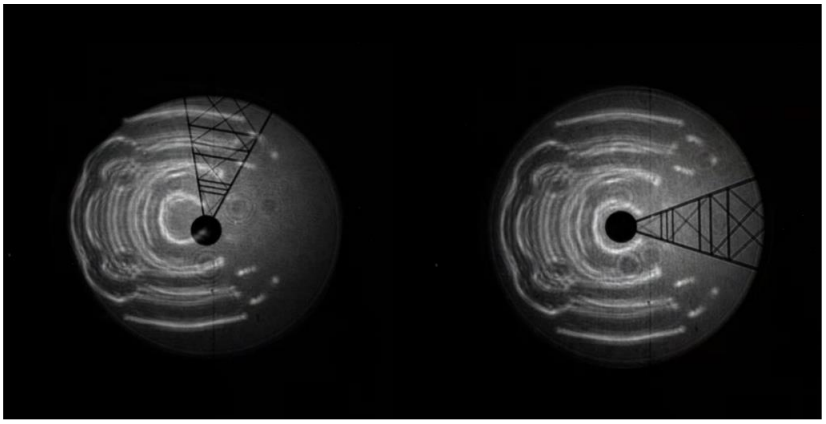

Figure 13: a super-position of LBT pupil image and SP1 before and after running the pupil alignment template. The displayed mis-alignment is exaggerated compared to realistic mis-alignment we will have to correct.

We started from different centering mis-alignment, to verify both the achieved precision in the final alignment and the necessary time to converge.
Results of tests are shown in *Table 5*. Each mis-alignment has been repeated at least 4 times, and the results shown are the average of all the iterations. It can be noticed that, for alignment to the apodizing masks, the algoritm always converge within the threshold in ~ 150s, independently from the initial mis-alignment. In all the cases the de-centering residual is well below the required 0.4%.

Table 5: results of pupil alignment routine starting from different initial mis-alignment. Associated error is the RMS of all the measurements. Consider that the alignment routine has a threshold of 0.2% of the pupil diameter to consider the alignment achieved; thus, the table has to be interpreted in this way: the achieved accuracy is always better than the threshold, and it is independent from the initial mis-alignment.

Initial mis-alignment [% pup. Diam.]	*Final mis-alignment [% pup. Diam.]*	*Final rotation mis-alignment [deg]*	*Elapsed time [s]*
0.49	0.07 ± 0.07	0.09 ± 0.10	149
1	0.12 ± 0.07	0.09 ± 0.07	149
2.18	0.06 ± 0.05	0.06 ± 0.07	155

5.2 Alignment routine telescope psf to occulting masks

This routine automatically acquire an image of the star PSF and of the occulting mask that will be used for the observation, and compute the centers of both. Acting on the tip-tilt of the internal DM, the star PSF position will be adjusted till the two images will be co-centered within Δx: 0.2px, Δy: 0.2 px, corresponding to ~ 3.5 μm of mutual shift at the CORO focal plane.

Requirement for psf centering calibration residual is 3 μm

Test was performed running 10 times the alignment routine and measuring the residual misalignment between the focal plane mask and the PSF. Starting from a reasonable misalignment between PSF and occulting mask of ~ 50 *mas* on sky, the alignment algorithm converges in ~ 50s with a maximum residual mis-alignment of 2.6 μm at CORO-FP, corresponding to 3 *mas* on sky. Larger initial misalignment would affect only the routine converging time, while the accuracy is maintained, since the routine has a threshold on the accepted alignment.

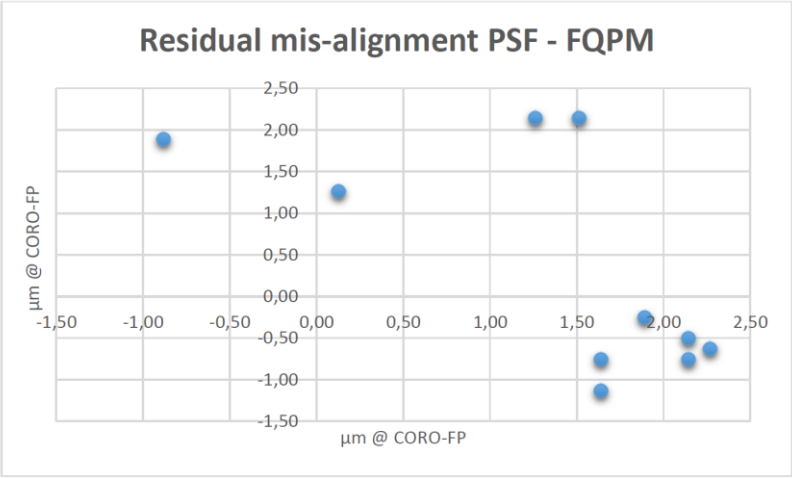

Figure 14: residual mis-alignments, in μm at the CORO-FP, between the PSF and the FQPM

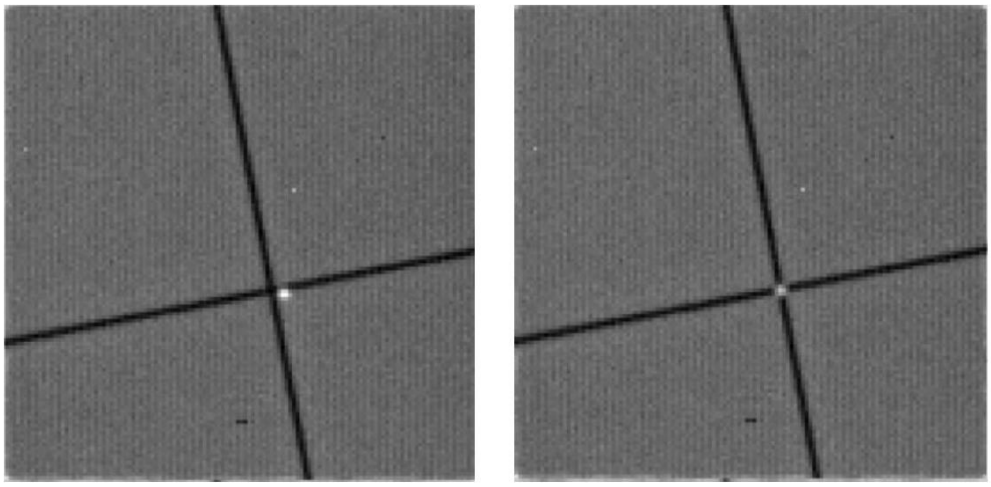

Figure 15: left panel, PSF is misaligned by 50 mas w.r.t the center of the FQPM. Right panel, PSF aligned to the center of the FQPM after running the alignment routine. Residual displacement is 3mas on sky.

6. PRE-COMMISSIONING RUN#1

SHARK-NIR successfully passed the PAE in March 2022 and was shipped to LBT in June 2022, with the first pre commissioning run started on June 25 and finished on July 12. [17][18]
Main scope of this run was verifying that the instrument did not need any major re-alignment after transportation and verify that it was still functioning and performing as in Padova.
Moreover, before reaching the telescope, SHARK-NIR SCICAM underwent some intervention at Steward Observatory to verify the cause of some excessive flexures of the SCICAM noticed during the flexures tests, so the effect of this intervention has been verified at the telescope. Teflon washers/screw that hold the detector to the mounting plate seemed to be a little loose, which might explain the movement of the detector.
These Teflon washers were replaced with another material and all has been reassembled and re-torqued and a dab of 2216 was applied so that they will not loosen with thermal cycling. Also 2216 was used on all other hardware to insure no more loosening of hardware with thermal cycling.
Finally, we upgraded the instrument to make Phase Diversity measurements more robust, adding two new lenses to the apodizers wheel. Now we are able to acquire 6 images of the PSF with 6 different defocus, adding way more constraints to the PD reconstructions. [19]

6.1 Optical quality

Optical quality, measured with Phase Diversity after optimization adding the 2 new defocusing lenses (see Section 6.3), was consistent with what was measured in Padova, with a residual WFE of the order of 30 nm, corresponding to a Strehl of 0.97 in Y band. Major contributions came from trefoil (visible in the PSF below) and Astigmatism.

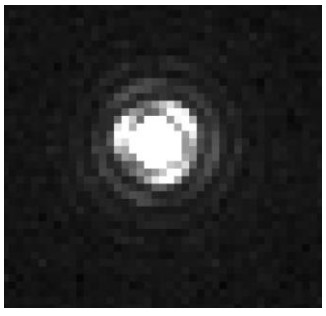

Figure 16: the on-axis PSF of SHARK-NIR after transportation. 30 nm of residual WFE were found by Phase Diversity.

6.2 SCICAM flexures verification

At the telescope we could not perform the whole flexures test campaign, due to lack of the needed equipment, especially the flexures handling. We thus compared the measured flexures in just one configuration, meaning with the bearing rotation axis parallel to the ground and with the bench rotating 180deg.

Referring to *Figure 17* we should compare the blue curve in the left panel with the yellow curve in the right panel. They basically represent the results of the same test (thus shift of the on-axis PSF on the SCICAM for a bearing rotation of 180°) in Padova (left panel) and at the telescope, after intervention at Steward Observatory (right panel).

We can see that the maximum excursion diminished from a value of ~ 400µm to ~ 270µm for a 180° bearing rotation. We know from flexures tests that this contribution will diminish more and more as the bearing rotation angle will be parallel to gravity vector. When SHARK-NIR will be mounted at the telescope and the telescope pointing at Zenith, the bearing rotation axis will have an inclination of ~30deg w.r.t. gravity vector.

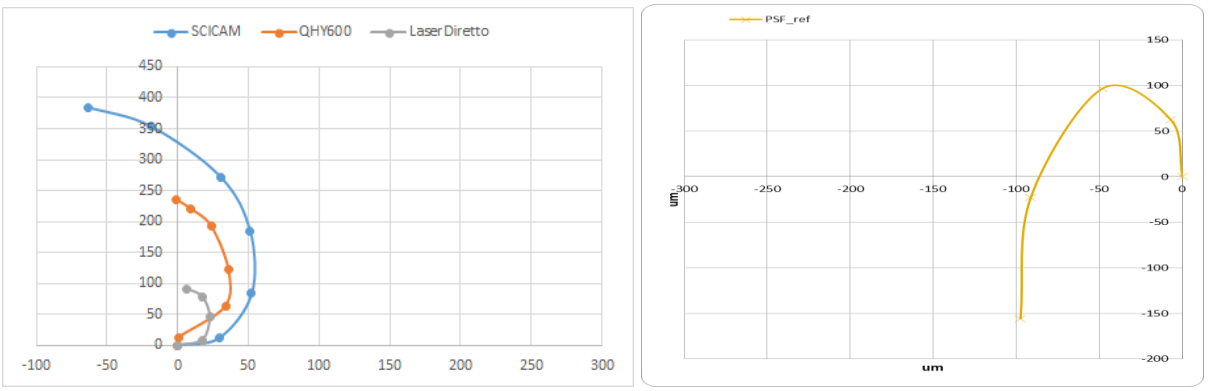

Figure 17: left panel (blue curve), the shift of the on-axis PSF during a 180deg rotation of the bearing, with bearing rotation axis parallel to the ground. Right panel, same test but after intervention on the SCICAM at Steward Observatory.

6.3 Optimized Phase Diversity measurement

After installation of the 2 new defocusing lenses, PD has been tested for the first time combining the internal fibers with these two new lenses. We were able to inject in this way up to 6 defocus amounts (in-focus case included). Results are promising, reconstructions seems to be more robust than in Padova. We acquired push-pull data from mode Z7 up to Z21 in order to build a reconstruction matrix. This matrix has been successfully used to convert PD modal output into DM commands.

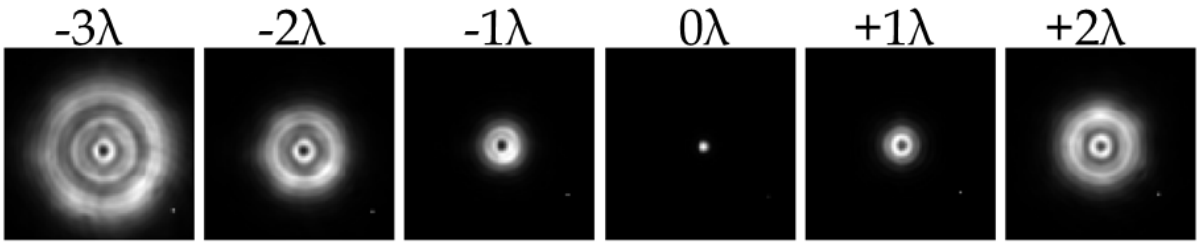

Figure 18: the 6 PSF with 6 different amount of defocus used for optimized PD.

In order to calculate the reconstructor we push-pulled each aberration with an amplitude of 50nm RMS of shape applied to the DM, below is the PD reconstructed wavefront. All the aberrations were correctly retrieved by PD, second order aberrations are mainly seen as primary aberrations but this was expected also from Zemax simulations.

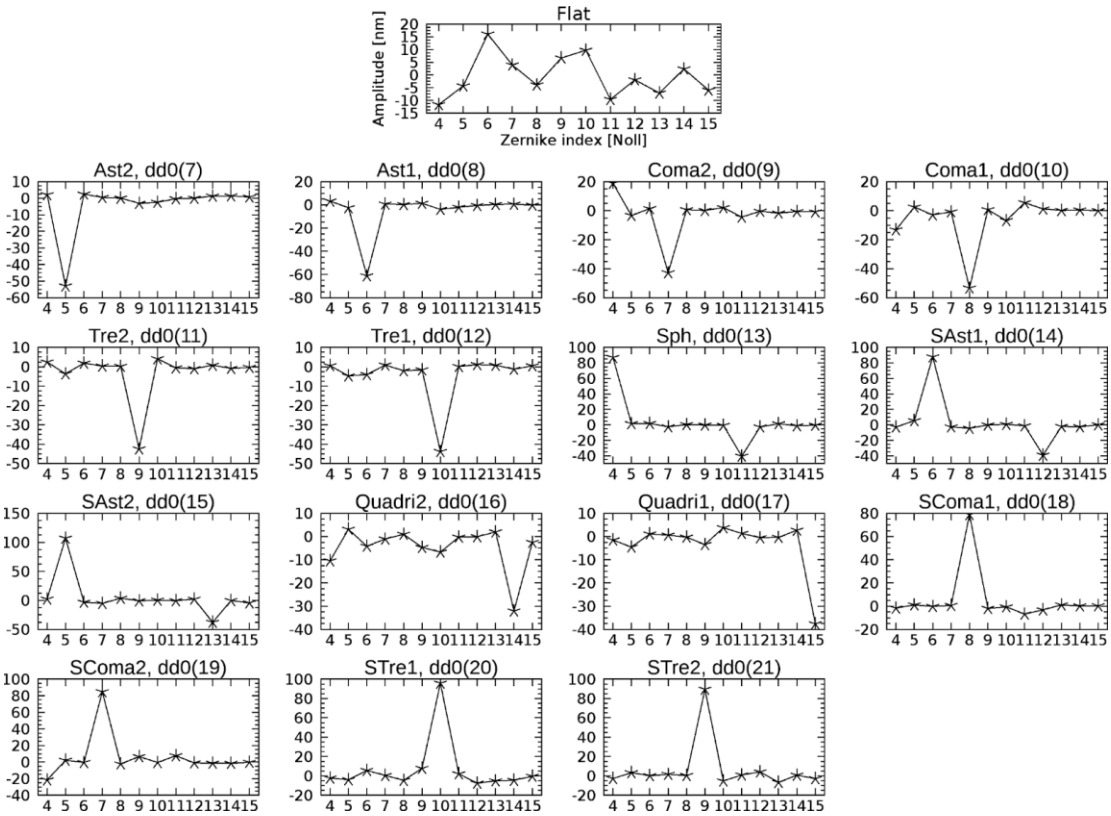

Figure 19: Phase Diversity reconstructed wavefront for each aberration, after flat subtraction. Caption of each graph indicates the commanded aberration to DM. Second order aberrations are mainly seen as primary order aberrations. Y-axis shown nm RMS of WFE, while X-axis shows the Noll coefficient # of the aberrations.

Nevertheless, we were also able to remove second order aberrations from the wavefront, as visible in *Figure 20.*

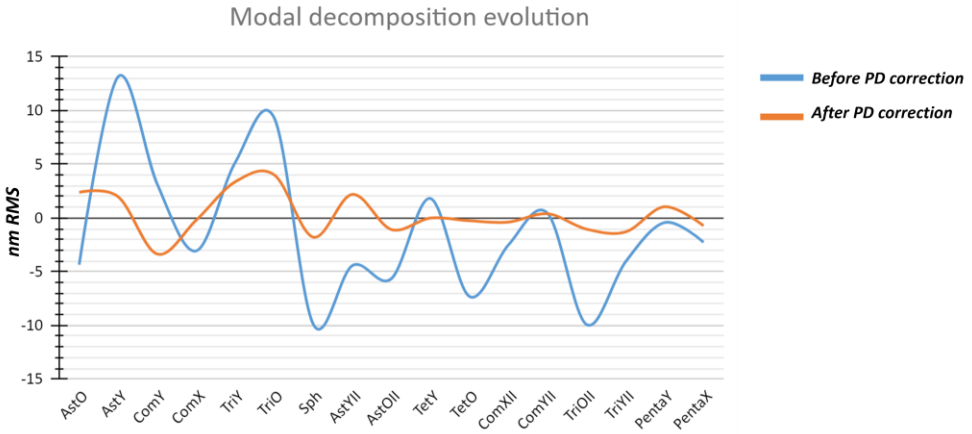

Figure 20: modal decomposition of WF before and after PD reconstruction.

Optical quality improved, the residual WFE diminished from 30 nm to less than 8 nm, meaning a Strehl > 0.99 in Y band. Measurements of PD proved to be very repeatable throughout the whole Pre-Com Run#1

Figure 21: residual WFE before and after PD correction.

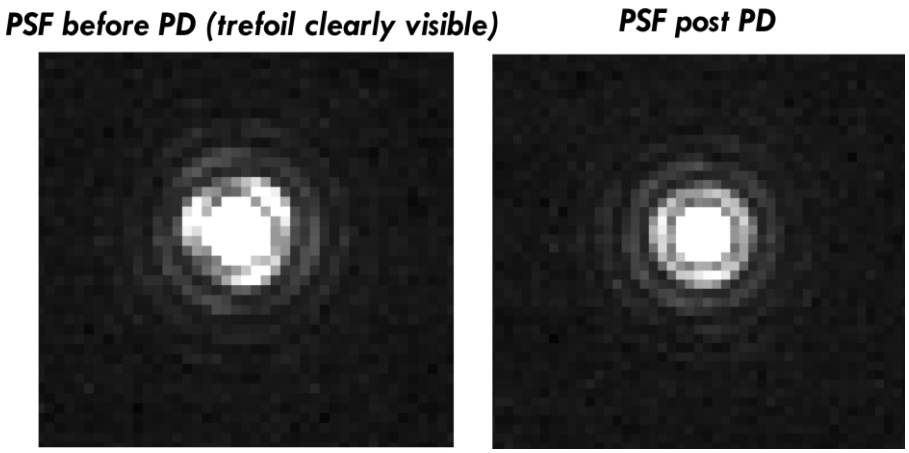

Figure 22: left panel the PSF before PD correction, right panel the PSF after PD correction.

REFERENCES

[1] Farinato, J.; Pedichini, F.; Pinna, E.; Baciotti, F.; Baffa, C.; Baruffolo, A.; Bergomi, M.; Bruno, P.; Cappellaro, E.; Carbonaro, L.; Carlotti, A.; Centrone, M.; Close, L.; Codona, J.; Desidera, S.; Dima, M.; Esposito, S.; Fantinel, D.; Farisato, G.; Fontana, A.; Gaessler, W.; Giallongo, E.; Gratton, R.; Greggio, D.; Guerra, J. C.; Guyon, O.; Hinz, P.; Leone, F.; Lisi, F.; Magrin, D.; Marafatto, L.; Munari, M.; Pagano, I.; Puglisi, A.; Ragazzoni, R.; Salasnich, B.; Sani, E.; Scuderi, S.; Stangalini, M.; Testa, V.; Verinaud, C.; Viotto, V.; "SHARK (System for coronagraphy with High order Adaptive optics from R to K band): a proposal for the LBT 2nd generation instrumentation", SPIE Proc. 9147, id. 91477J 10 pp. (2014).

[2] Hill, J. M. and Salinari, P., "Large Binocular Telescope project," Proc. SPIE, 4004, 36–46 (2000).

[3] Mattioli M., Pedichini F., Antoniucci S., Li Causi G., Piazzesi R., Stangalini M., Testa V., "SHARK-VIS the LBT high contrast imager at visible wavelengths", SPIE Proc., Volume 10702 (2018)

[4] Farinato, J., Baffa, C., Baruffolo, A., Bergomi, M., Carbonaro, L., Carlotti, A., Centrone, M., Codona, J., Dima, M., Esposito, S., Fantinel, D., Farisato, G., Gaessler, W., Giallongo, E., Greggio, D., Hink, P., Lisi, F., Magrin, D., Marafatto, L., Pedichini, F., Pinna, E., Puglisi, A., Ragazzoni, R., Salasnich, B., Stangalini, M., Verinaud, C. and Viotto, V., "The NIR arm of SHARK (System for coronagraphy with High order Adaptive optics from R to K band)", International Journal of Astrobiology, 14(3), 365-373 (2015)

[5] Esposito, S., Riccardi, A., Pinna, E., Puglisi, A. T., Quirós-Pacheco, F., Arcidiacono, C., Xompero, M., Briguglio, R., Busoni, L., Fini, L., Argomedo, J., Gherardi, A., Agapito, G., Brusa, G., Miller, D. L., Guerra Ramon, J. C., Boutsia, K. and Stefanini, P. "Natural guide star adaptive optics systems at LBT: FLAO commissioning and science operations status", Proc. SPIE, 8447, 84470U (2012)

[6] Ragazzoni, R., "Pupil plane wavefront sensing with an oscillating prism," Journal of Modern Optics 43, 289 (1996).

[7] Riccardi, A.; Xompero, M.; Briguglio, R.; Quirós-Pacheco, F.; Busoni, L.; Fini, L.; Puglisi, A.; Esposito, S.; Arcidiacono, C.; Pinna, E.; Ranfagni, P.; Salinari, P.; Brusa, G.; Demers, R.; Biasi, R.; Gallieni, D.; "The adaptive secondary mirror for the Large Binocular Telescope: optical acceptance test and preliminary on-sky commissioning results", SPIE 7736, 79 (2010)

[8] Hinz, P.M., Angel, J.R.P., McCarthy, D.W., Hoffman, W.F., and Peng, C.Y., "The large binocular telescope interferometer," in Proc. SPIE, 4838, 108 (2003).

[9] Pinna, E., Pedichini, F., Farinato, J., Esposito, S., Centrone, M., Puglisi, A., Carbonaro, L., Agapito, G., Riccardi, A., Xompero, M., Hinz, P., Montoya, M., and Bailey, V., "XAO at LBT: current performances in the visible and upcoming upgrade," Proc. of AO4ELT4 conference (2015)

[10] Ragazzoni, R.; Farinato, J.; "Sensitivity of a pyramidic Wave Front sensor in closed loop Adaptive Optics", A&A, 350, L23 (1999)

[11] Vérinaud, C.; Le Louarn, M.; Korkiakoski, V.; Carbillet, M.; "Adaptive optics for high-contrast imaging: pyramid sensor versus spatially filtered Shack-Hartmann sensor", MNRAS, 357, L26 (2005)

[12] Esposito, S.; Riccardi, A.; "Pyramid Wavefront Sensor behavior in partial correction Adaptive Optic systems", A&A, 369, L9 (2001)

[13] Costa, Joana B.; Feldt, Markus; Wagner, Karl; Bizenberger, Peter; Hippler, Stefan; Baumeister, Harald; Stumpf, Micaela; Ragazzoni, Roberto; Esposito, Simone; Henning, Thomas; "Status report of PYRAMIR: a near-infrared pyramid wavefront sensor for ALFA", SPIE Proc. 5490, 1189 (2004)

[14] Viotto V., Ragazzoni R., Bergomi M., Farinato J. "Expected gain in the pyramid wavefront sensor with limited Strehl ratio", A&A, Volume 593 (2016)

[15] Beuzit, J.-L.; Boccaletti, A.; Feldt, M.; Dohlen, K.; Mouillet, D.; Puget, P.; Wildi, F.; Abe, L.; Antichi, J.; Baruffolo, A.; Baudoz, P.; Carbillet, M.; Charton, J.; Claudi, R.; Desidera, S.; Downing, M.; Fabron, C.; Feautrier, P.; Fedrigo, E.; Fusco, T.; Gach, J.-L.; Giro, E.; Gratton, R.; Henning, T.; Hubin, N.; Joos, F.; Kasper, M.; Lagrange, A.-M.; Langlois, M.; Lenzen, R.; Moutou, C.; Pavlov, A.; Petit, C.; Pragt, J.; Rabou, P.; Rigal, F.; Rochat, S.; Roelfsema, R.; Rousset, G.; Saisse, M.; Schmid, H.-M.; Stadler, E.; Thalmann, C.; Turatto, M.; Udry, S.; Vakili, F.; Vigan, A.; Waters, R.; "Direct Detection of Giant Extrasolar Planets with SPHERE on the VLT", ASP Proc. 430, 231 (2010)

[16] Macintosh, B. A., Graham, J. R., Palmer, D. W., Doyon, R., Dunn, J., Gavel, D. T., Larkin, J., Oppenheimer, B., Saddlemyer, L., Sivaramakrishnan, A., Wallace, J. K., Bauman, B., Erickson, D. A., Marois, C., Poyneer, L. A., and Soummer, R., "The Gemini Planet Imager: from science to design to construction," Proc. SPIE 7015, 31 (2008).

[17] M. Bergomi, L. Marafatto, E. Carolo, D. Greggio, D. Ricci, D. Vassallo, L. Lessio, K. K. Radhakrishnan Santhakumari, G. Umbriaco, M. Dima, S. Di Filippo, V. D'Orazi , D. Mesa, M. Montoya, L. Mohr, V. Viotto, A. Baruffolo, F. Biondi, S. Chavana, S. Chinellato, M. De Pascale, K. W. Don, P. Grenz, F. Laudisio, J. Leisenrin , R. Ragazzoni, F. Pedichini, R. Piazzesi, E. Pinna, A. Puglisi, A. Bianco, A. Carlotti, C. Knapic, M. Vicinanza, A. Zanutta, J. Christou, A. Conrad, L. Funk, C. Veillet, J. Farinato., "SHARK-NIR: from design to installation, ready to dive into first light", Proc.SPIE 12187-8 (2022)

[18] Jacopo Farinato, Andrea Baruffolo, Maria Bergomi, Andrea Bianco, Federico Biondi, Elena Carolo, Alexis Carlotti, Sona Chavan, Simonetta Chinellato, Marco De Pascale, Marco Dima, Valentina D'Orazi, Steve Ertel, Davide Greggio, Thomas Henning, Fulvio Laudisio, Luigi Lessio, Demetrio Magrin, Luca Marafatto, Dino Mesa, Lars Mohr, Manny Montoya, Kalyan Radhakrishnan, Davide Ricci, Gabriele Umbriaco, Daniele Vassallo, Valentina Viotto, Alessio Zanutta, Simone Antoniucci, Carmelo Arcidiacono, Francesca Bacciotti, Pierre Baudoz, Angela Bongiorno, Laird Close, Simone Di Filippo, Simone Esposito, Paul Grenz, Olivier Guyon, Jarron M. Leisenring, Fernando Pedichini, Roberto Piazzesi, Enrico Pinna, Elisa Portaluri, Alfio Puglisi, Roberto Ragazzoni, Fabio Rossi, "SHARK-NIR, ready to "swim" in the LBT northern hemisphere "ocean" " Proc. SPIE 12185, (2022)

[19] Daniele Vassallo, Maria Bergomi, Elena Carolo, Davide Greggio, Luca Marafatto, Gabriele Umbriaco, Jacopo Farinato, Andrea Baruffolo, Kalyan Kumar Radhakrishnan Santhakumari, Valentina Viotto, Jean-François Sauvage, Thierry Fusco, "Laboratory demonstration of focal plane wavefront sensing using phase diversity: a way to tackle the problem of NCPA in SHARK-NIR. Part II: New characterization tests and alternative wavefront sensing strategies" Proc. SPIE 12185 (2022)